Competing phases of the Hubbard model on a triangular lattice – insights from the entropy

Gang Li,¹ Andrey E. Antipov,^{2,3} Alexey N. Rubtsov,⁴ Stefan Kirchner,^{2,3} and Werner Hanke¹

¹Institut für Theoretische Physik und Astrophysik, Universität Würzburg, 97074 Würzburg, Germany

²Max Planck Institute for Chemical Physics of Solids, 01187 Dresden, Germany

³Max Planck Institute for the Physics of Complex Systems, 01187 Dresden, Germany

⁴Department of Physics, Moscow State University, 119992 Moscow, Russia

Based on the ladder dual-fermion approach, we present a comprehensive study of the phases of the isotropic Hubbard model on the triangular lattice. We find a rich phase diagram containing most of the phases that have already been experimentally observed in systems where the interplay between geometric frustration and electronic correlations is important: paramagnetic metal, paramagnetic insulator, Mott-insulator with 120° antiferromagnetic and a non-magnetic insulating state, i.e. possibly a spin liquid state. This establishes that the Hubbard model on frustrated lattices can serve as a minimal model to address the intricate interplay of frustration and correlation. We also show that entropic considerations can be successfully used for understanding many striking features of the triangular systems, such as the large thermopower found in $Na_xCoO_2 \cdot yH_2O$.

PACS numbers: 71.10.Fd, 71.27.+a, 71.30.+h

Introduction. Spin models with frustrated interactions, caused either by geometric frustration of the underlying lattice or due to competing interactions, can differ significantly in their physical properties from their nonfrustrated counterparts. In a frustrated system, a spin cannot find a configuration that simultaneously minimizes all its interactions with its neighbors. As a result, spin frustration may completely suppress the longrange magnetic ordering in a system, resulting in a nonmagnetic insulating ground state that does not break any symmetry, i.e. a spin liquid (SL) state [1]. Real magnetic materials are typically characterized by frustrated interactions which give rise to rich phase diagrams. A SL state, may have been observed e.g. the organic salts κ -(BEDT-TTF)₂Cu₂(CN)₃ [2], where the frustration among the quantum spins is due to the underlying triangular lattice. In contrast, the organic charge transfer salt κ -(BEDT-TTF)₂Cu[N(CN)₂]Cl displays anti-ferromagnetic (AF) long-range order at low temperatures [3]. The κ -(BEDT-TTF)₂X family and the layered cobaltate Na_xCoO₂·yH₂ are triangular systems that give rise to superconductivity (SC) [4-6]. It is an open question if the emergence of SC in these systems can be connected to the SC phases observed in the high-T_c cuprates. Moreover, these systems also display Fermiliquid behavior and give rise to Mott insulating behavior, as well as to transitions between a SL and antiferromagnet (AFM) [2, 7]. We also note that an unusually large thermopower is found in the cobaltate $Na_xCoO_2 \cdot yH_2$ [8].

The existence of electronic phases on frustrated lattices indicates the necessity to consider itinerant electron models as effective low energy models for these systems that allow for the interplay between electron correlation and geometric frustration. All materials mentioned above have an effective triangular structure and are characterized by strong electronic correlations. This raises the important question if Hubbard-type models on the triangular lattice constitute a model class that can encompass the experimentally observed phases as possible ground states.

In the present letter, we study the finite-temperature thermodynamic, electronic, and magnetic properties of the doped isotropic triangular Hubbard (ITH) model. The resulting phase diagram is summarized in Figs. (1)(a) (at half filling) and (2) (away from half filling). One standard approach to strongly correlated electronic systems is based on the dynamical mean-field theory (DMFT) [9]. The inclusion of the effects of geometric frustration, however, requires an extension beyond the single-site problem. Faithfully capturing the competition between strong correlations and geometric frustration across the phase diagram is not only essential but also very challenging. Our study is based on a powerful technique, *i.e.* the ladder dual-fermion approach (LDFA) [10].

The dual fermion approach [11] is a non-local extension of the DMFT. It introduces a set of dual variables with an effective interaction formed by the reducible two-particle vertex of the interacting fermions as obtained from the DMFT. An interaction expansion over the dual variables yields systematic non-local corrections to the standard DMFT approach. Studies have shown that already the inclusion of the first two lowest-order dual diagrams produces good agreement with numerically exact results [12]. Including higher order diagrams further improves the agreement [10]. In what follows, we take the hopping parameter t of the ITH as our unit of energy, i.e. t=1.

Our choice of method for addressing the ITH is motivated by the advantages it offers over possible alternatives: (1) the calculations are not restricted to finite-size clusters, *i.e.* the thermodynamic limit and nonlocal-

ity are naturally incorporated, (2) although a quantum Monte Carlo simulation is involved [13], the calculations are free of the "minus"-sign problem (everywhere in the phase diagram), (3) both spin and charge collective excitations are accessible which allows us to establish the nature of various insulating and magnetic phases. In what follows, we take the hopping parameter t of the ITH as our unit of energy, *i.e.* t=1.

Results. The magnetic phase diagram of the half-filled ITH model within our approach is shown in Fig. 1(a). In analogy to its counterpart on a square lattice [9, 14], three major phases are found for the ITH: a paramagnetic metal at smaller interaction U, a paramagnetic insulator at larger U and higher temperature T, and a Mott insulator with 120°-AF order at larger U and lower T.

As our finite-temperature LDFA calculations are carried out on discrete Matsubara frequencies, the exact location of the metal-insulator transition (MIT) boundary is hard to determine. In this work, we identify the first-order transition line from the flatness of $G_{ii}^{LDFA}(i\omega)$ at the two lowest Matsubara frequencies [15]. The magnetic transition boundary is extracted from the extrapolation of the inverse spin susceptibility $\chi_{\Omega_m=0}^{spin,-1}(\mathbf{Q}=\mathbf{K})$ as a function of temperature T and interaction U. (see examples in the supplemental material), where \mathbf{K} is the magnetic wave vector for the 120°-AF order.

The influence of geometrical frustration on the magnetic properties is clearly visible, see Fig. 1(a): the onset temperature of the 120° -AF (also called spiral-AF) state is significantly smaller than its counterpart for unfrustrated lattices (for the square lattice, this corresponds to the black dashed line of Fig. 1(a) [14]). While for the Hubbard model on a square lattice, AF order exists for any non-vanishing value of U, the geometrical frustration of the triangular system suppresses the long-range magnetic order at smaller U down to zero temperature, resulting in a non-magnetic metal below $U \sim 9.55$. Here, the onset temperature of the 120°-AF order (which is strictly speaking absent in 2D [16]), obtained from our calculations, can be viewed as the upper limit of the Néel temperature for a triangular system with a larger dimension, e.g. by coupling the triangular lattice into multilayers.

A very interesting effect of geometric frustration is that it pushes the magnetic transition boundary towards higher U values to a value close to U_c^{MIT} , opening up the possibility of a ground state characterized by a nonzero charge gap and the absence of any long-range magnetic order(see Fig. 1(a)). This is indeed what we find within the LDFA: there is a non-magnetic Mott insulating (NMI) phase in the interval $U \in [9.4, 9.55]$ for $T \leq 0.08$ [18]. The appearance of the NMI phase is highlighted by the crossing of magnetic and insulating phase boundaries in Fig. 1(a). We find for the critical value $U_c^{MIT} = 9.4$ at T = 0.2 and U_c^{MIT} hardly changes upon further decreasing T. The magnetic transitions

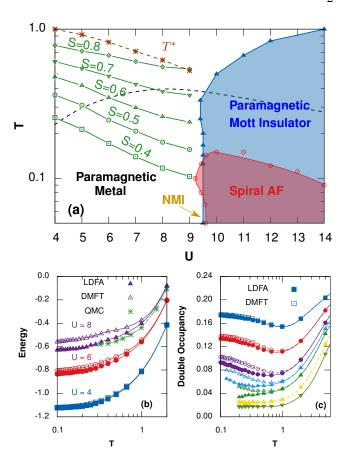


FIG. 1. (a). T-U phase diagram of the half-filled ITH model. The monotonic decrease of the constant-entropy curve reveals the possibility of adiabatic cooling in this frustrated system. T^* is the corresponding temperature at which the double occupancy in Fig. 1(c) is minimized. The NMI phases are found at lower temperature region ($T \leq 0.08$) and for U slightly larger than the band width ($U \in [9.4, 9.55]$). See text for more details. (b). Comparison of the total energy $E_U(T)$ calculated from the DMFT (empty symbols) and the LDFA (solid symbols) calculations. Their difference results from the non-local correlations. The QMC results for U = 8 are extracted from Ref. [17]. (c). The double occupancy as a function of temperature for different interactions (From top to bottom: U = 4, 6, 8, 9, 10, 12, 14, respectively.)

sition from the paramagnetic to the 120°-AF state, on the other hand, shows a clear temperature dependence, i.e. U_c^{Spin} becomes larger with lowering the temperature for $T \leq 0.11$. At the lowest temperature studied $(T_{\text{low}} = 0.05)$, long-range order is established at U = 9.55, leaving the phase with $U \in [9.4, 9.55]$ to be a NMI. Note that this conclusion is free of any finite-size effects but the phase boundaries in Fig. 1(a) are subject to extrapolations (see supplemental material). The NMI is a natural candidate for the SL phase at zero-temperature and our results are in line with experimental findings for κ -(BEDT-TTF)₂Cu₂(CN)₃ [2]. The bulk spin susceptibility of κ -(BEDT-TTF)₂Cu₂(CN)₃ shows no sign of long-range antiferromagnetic order at significantly lower

temperature as compared to the Heisenberg exchange estimated theoretically from the high-temperature series expansion [19].

In order to assess the importance of non-local correlations, we analyze the total energy $E_U(T)$ for the ITH within DMFT-only and LDFA calculations, see Fig. 1(b). The difference between the DMFT and the LDFA solutions at fixed T signals the importance of non-local fluctuations, which is particularly large when U is close to U_c^{MIT} . Note that $E_U(T)$ from DMFT is never smaller than the one obtained from the LDFA. At U = 8, the LDFA results show a good agreement with a determinant QMC simulation [17] for all temperatures sampled. Thus, our LDFA calculations systematically incorporate non-locality into DMFT and correctly resolve the total energy at low temperatures. At low temperatures the DMFT results clearly differ from the determinant QMC results. Thus, Fig. 1(b) demonstrates that non-local correlations are significant and cannot be neglected. These correlations stabilize the *Mott* insulating phase [20–22] and suppress spin correlations [23, 24], thereby favoring the NMI phase at lower temperatures.

Another important observation that can be read off from Fig. 1(a) is, that the constant-entropy curves monotonically decrease with increasing U. The entropy is obtained from the total energy by integration, i.e. $S_U(T,n)=S(0,n)+E_U(T,n)/T-\int_T^\infty E_U(T')/T'^2dT',$ with $S(0,n)=-n\ln n/2-(2-n)\ln(1-n/2),$ where n is the average filling. For numerical stability, we fitted the total energy $E_U(T)$ with an exponential function [25] and also cross-checked with a two-segment fitting scheme [17, 26], which resulted in the same qualitative behavior of $S_U(T)$. The entropy is related to the number of doubly occupied sites D through a thermodynamic relation, i.e. $\partial S/\partial U = -\partial D/\partial T$. As shown in Fig. 1(c), the double occupancy D has a negative slope for temperatures below the critical value T^* , thus, resulting in an increase of S as U increases for fixed T(Fig. 1(a)). This has important ramification for coldatom studies in that it allows for adiabatic cooling of the system by increasing the Coulomb interaction [27, 28].

The relation above can be rewritten $C/T(\partial T/\partial U)_S = (\partial D/\partial T)_T$ where C denotes the specific heat. This immediately implies that the isentropic (i.e. keeping the entropy constrant) increase of U results in a decrease of T for $T \leq T^*$. As one can see from Fig. 1(a), the decreasing behavior of the entropy ends at T^* . This is due to the opening of the charge gap, resulting in a saturation of D at lower temperatures [27]. The T^* curve (by extrapolation) ends at the boundary of the insulating phase in Fig. 1(a). We note that the insulating phase boundary in Fig. 1(a) is determined from the opening of the charge gap, which, as expected, coincides with the saturation of D (see Fig. 1(c)) in our LDFA calculations.

We now turn to the doping dependence away from half-

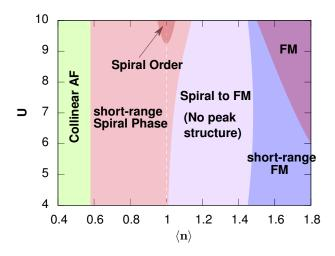


FIG. 2. Magnetic phase diagram of the doped triangular Hubbard model as a function of the Coulomb strength at T=0.1. Two stable magnetic phases are found, *i.e.* a spiral(120°)-AF (anti-ferromagnetic) and a ferromagnetic (FM) phase. Shortranged 120° -AF and FM states are found in the vicinity of long-range 120° -AF and FM phases.

filling. Fig. 2 displays the magnetic phase diagram of the ITH model as a function of doping and U. As discussed in Fig. 1(a), the 120°-AF phase is stabilized at T=0.1 for U>9.5 at half filling (i.e. $\langle n\rangle=1$). This phase extends slightly away from the half-filling case, as shown in Fig. 2. The stability of the 120°-AF phase is characterized by the divergence of $\chi^{spin}_{\Omega_m=0}(\mathbf{Q})$ at $\mathbf{Q}=\mathbf{K}$. By doping the system away from half-filling, the spiral-AF phase is quickly destroyed, resulting in a very narrow phase region (see Fig. 2).

At the electron doped side, the destruction of the 120°-AFM is characterized by the removal of the spin susceptibility peak at **K**. As shown in Fig. 3(d), at $\langle n \rangle = 1.1$, the spin susceptibility peak at $\mathbf{Q} = \mathbf{K}$ starts to disappear. Further increasing electron doping completely removes the peak, giving rise to a flat structure of $\chi_{\Omega_m=0}^{spin}(\mathbf{Q})$ at \mathbf{Q} around \mathbf{K} (Fig. 3(e)). This region extends approximately from $\langle n \rangle = 1.1$ to $\langle n \rangle = 1.45$ (see Fig. 2) and corresponds to a crossover from an 120°-AF to a ferromagnetic (FM) phase. In this region, no peak structure has been detected in the spin susceptibility; these states are paramagnetic. A further increase of the doping level results in a peak in the spin susceptibility at $\mathbf{Q} = \mathbf{\Gamma}$. as shown in Fig. 3(f), indicating the formation of FM correlations. The divergence of $\chi^{spin}_{\Omega_m=0}(\Gamma)$ represents the onset of a stable FM phase.

At the hole doped side, however, the destruction of $\chi^{spin}_{\Omega_m=0}(\mathbf{K})$ as the hole concentration is increased, occurs much slower. We find a large region of $\chi^{spin}_{\Omega_m=0}(\mathbf{K})$ with peak structure, which spreads from $\langle n \rangle \sim 1.0$ to $\langle n \rangle \sim 0.55$. This is in a sharp contrast to the electron doped side, where $\chi^{spin}_{\Omega_m=0}(\mathbf{K})$ is quickly destroyed and

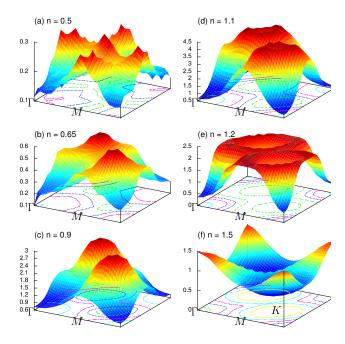


FIG. 3. Spin susceptibilities $\chi^{spin}_{\Omega_m=0}(\mathbf{Q})$ extracted from the LDFA scheme for six different doping levels and $\beta=10$, U=W with W the bandwidth. Γ , \mathbf{M} and \mathbf{K} are the high-symmetry points of the 1st BZ of the triangular lattice. The 1st BZ is replotted here equivalently as a square.

absent for $\langle n \rangle$ above $\langle n \rangle \sim 1.1$. In accordance with the suppression of $\chi^{spin}_{\Omega_m=0}$ at \mathbf{K} , the amplitude of $\chi^{spin}_{\Omega_m=0}(\mathbf{M})$ gradually increases. This indicates that scattering processes with magnetic wave vector $\mathbf{Q} = \mathbf{M}$ have larger and larger contributions, while those with $\mathbf{Q} = \mathbf{K}$ become less important. Increasing the hole doping further, $\chi^{spin}_{\Omega_m=0}(\mathbf{M})$ starts to peak at around $\langle n \rangle \sim 0.5$. This behavior corresponds to AF states of the collinear type (CAF).

The observation of CAF in an isotropic system on a non-bipartite lattice is rather unexpected. While it has been established that spin anisotropy in Heisenberg models on the triangular lattice favors CAF [29], it usually requires higher order hopping processes in an isotropic triangular lattice to bring about a CAF phase [30]. In this work, we provide another alternative way of obtaining CAF in *isotropic* triangular lattice, namely doping the system with holes. The present case does, however, differ from the previously discussed cases [29, 30] as no long-range magnetic order is observed here. Another essential difference is that hole doping turns the system metallic while the system is insulating in the previous cases.

The entropy S of the doped triangular system is shown in Fig. 4(a). We determine the entropy by using the same procedure as for the half-filled case. The calculation has been performed with U fixed at U=9, which is only slightly below U_c^{MIT} where the system enters into a mag-

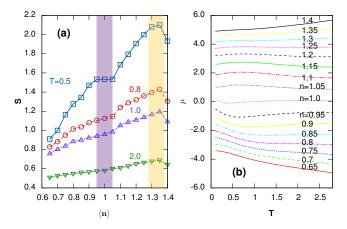


FIG. 4. (a) The doping dependence of the entropy for four different temperatures with U=W. The two color filled area show the entropy plateau at half-filling and maximization at $\langle n \rangle \sim 1.35$. (b) Temperature dependence of the chemical potential for a range of filling levels. From bottom to top, the curves correspond to n=0.65 to n=1.4 with 0.05 as interval.

netically ordered Mott insulating state. Thus, spin and charge fluctuations are enhanced and contribute significantly to S. In Fig. 4(b), we show the chemical potential μ vs. T at various levels of fillings. S and μ are related via the Maxwell relation $(\partial S/\partial n)_{T,U} = -(\partial \mu/\partial T)_{U,n}$. The chemical potential shows opposite behavior (decreasing versus increasing) at hole- and electron-doped sides (see Fig. 4(b)). Correspondingly, the entropy displays different filling dependencies with respect to electrons and holes. As already can be read off from Fig. 2, the strong AF correlations are destroyed quickly when doping the half-filled system with electrons but persist to a large level of hole doping. This is reflected in the behavior of S, which on the hole-doped side is smaller than on the electron-doped one. We note that the Hubbard model on a square lattice displays a similar behavior, but with the opposite electron and hole dependence [31]. This implies certain similarities between the square and triangular lattice. S shows a plateau around half-filling, which relates to the nearly constant μ for all temperatures at half-filling ($\langle n \rangle = 1$).

Motivated by the fact that S in the Hubbard model on the square lattice becomes maximal near optimal doping, i.e. $\langle n \rangle \approx 0.85$, where the SC transition temperature is peaked [26, 32]. we locate the filling on the triangular lattice that maximizes S. Interestingly, the thus obtained 'optimal' filling for the triangular system, $\langle n \rangle \sim 1.35$ coincides well with the optimal filling found in Na_xCoO₂·1.3H₂O [5, 6, 33]. The maximization of the entropy reflects the strong competition of the localized spin degrees of freedom (around half-filling) with the charge degrees of freedom (here at large electron doping). Enhanced entropy commonly occurs in the vicinity

of quantum critical points. In line with what is seen in the cuprates [34] we, therefore, speculate that the ground state of the ITH model may have a quantum critical point at this filling. We will return to this issue in future work.

Our results of the filling dependence of S allow us to estimate the Seebeck coefficient via Kelvin's formula, $S_{kelvin} = 1/q_e(\partial S/\partial n)_{T,U}$ [35]. We find that the thermopower is large (negative) at $\langle n \rangle \sim 1.5$ but rather smaller at $\langle n \rangle \sim 1.35$. This nicely explains the different doping behaviors of the thermopower experimentally found in Na_xCoO₂·1.3H₂O [6, 36]. When $\langle n \rangle$ is larger than 1.3, S starts to decrease with a large negative slope, which coincides with the large thermopower at $\langle n \rangle \sim 1.5$ in Na_xCoO₂·1.3H₂O.

In conclusion, we studied the isotropic triangular Hubbard model using the dual fermion approach to systematically incorporate non-local correlations beyond the DMFT. By varying temperature, Coulomb interaction, and chemical potential, we find that this model gives rise to a very rich phase diagram, which recovers all the phases experimentally resolved in organic salts and the recently much-studied layered cobaltate $Na_xCoO_2 \cdot 1.3H_2O$ (we do not explicitly calculate the SC phase). Moreover, based on the behavior of the entropy, we find that the isotropic triangular Hubbard model displays certain similarities to the Hubbard model on square lattice for cuprates. Specifically, we find that the entropy is maximal at the optimal doping for superconductivity of $Na_xCoO_2\cdot 1.3H_2O$, and the experimentally observed different thermopower behaviors can be nicely explained by the doping dependence of the entropy through the Kelvin formula.

Acknowledgments: We acknowledge the stimulating post (at Nov. 09, 2011) of Ross H. McKenzie in his blog "CONDENSED CONCEPTS" [37], which inspired our discussion on the chemical potential and the entropy vs. filling. We thank F. Assaad and M. Katsnelson for fruitful discussions. G.L. and W.H. are financially supported by DPG Grant Unit FOR1162. One of us (W.H.) acknowledges the hospitality of the KITP at the university of California in Santa Barbara, where part of this work was completed and supported by the NSF under Grant No. NSF PHY11-25915. A.N.R. acknowledges the RFFI grant 11-02-01443, Dynasty foundation and S.K. the support under NSF Grant No. PHYS-1066293 and the hospitality of the Aspen Center for Physics.

- [1] L. Balents, Nature (London) 464, 199 (2010).
- [2] Y. Shimizu, K. Miyagawa, K. Kanoda, M. Maesato, and G. Saito, Phys. Rev. Lett. 91, 107001 (2003).
- [3] P. Limelette, P. Wzietek, S. Florens, A. Georges, T. A. Costi, C. Pasquier, D. Jérome, C. Mézière, and P. Batail, Phys. Rev. Lett. 91, 016401 (2003).
- [4] K. Takada, H. Sakurai, E. Takayama-Muromachi,

- F. Izumi, R. A. Dilanian, and T. Sasaki, Nature **422**, 53 (2003).
- [5] R. E. Schaak, T. Klimczuk, M. L. Foo, and R. J. Cava, Nature 424, 527 (2003).
- [6] M. L. Foo, Y. Wang, S. Watauchi, H. W. Zandbergen, T. He, R. J. Cava, and N. P. Ong, Phys. Rev. Lett. 92, 247001 (2004).
- [7] T. Itou, A. Oyamada, S. Maegawa, M. Tamura, and R. Kato, Phys. Rev. B 77, 104413 (2008).
- [8] M. Lee, L. Viciu, L. Li, Y. Wang, M. L. Foo, S. Watauchi, R. A. P. Jr, R. J. Cava, and N. P. Ong, Nature Materials 5, 537 (2006).
- [9] A. Georges, G. Kotliar, W. Krauth, and M. J. Rozenberg, Rev. Mod. Phys. 68, 13 (1996).
- [10] H. Hafermann, G. Li, A. N. Rubtsov, M. I. Katsnelson, A. I. Lichtenstein, and H. Monien, Phys. Rev. Lett. 102, 206401 (2009).
- [11] A. N. Rubtsov, M. I. Katsnelson, A. I. Lichtenstein, and A. Georges, Phys. Rev. B 79, 045133 (2009).
- [12] N. E. Bickers and S. R. White, Phys. Rev. B 43, 8044 (1991).
- [13] A. N. Rubtsov, V. V. Savkin, and A. I. Lichtenstein, Phys. Rev. B 72, 035122 (2005).
- [14] J. Kuneš, Phys. Rev. B 83, 085102 (2011).
- [15] R. Kovacik, P. Werner, K. Dymkowski, and C. Ederer, (2012), arXiv:1206.1423.
- [16] N. D. Mermin and H. Wagner, Phys. Rev. Lett. 17, 1133 (1966).
- [17] K. Aryanpour, W. E. Pickett, and R. T. Scalettar, Phys. Rev. B 74, 085117 (2006).
- [18] A. E. Antipov, A. N. Rubtsov, M. I. Katsnelson, and A. I. Lichtenstein, Phys. Rev. B 83, 115126 (2011).
- [19] W. Zheng, R. R. P. Singh, R. H. McKenzie, and R. Coldea, Phys. Rev. B 71, 134422 (2005).
- [20] E. Gull, P. Werner, X. Wang, M. Troyer, and A. J. Millis, EPL (Europhysics Letters) 84, 37009 (2008).
- [21] H. Park, K. Haule, and G. Kotliar, Phys. Rev. Lett. 101, 186403 (2008).
- [22] H. Lee, G. Li, and H. Monien, Phys. Rev. B 78, 205117 (2008).
- [23] G. Li, H. Lee, and H. Monien, Phys. Rev. B 78, 195105 (2008).
- [24] S. Brener, H. Hafermann, A. N. Rubtsov, M. I. Katsnelson, and A. I. Lichtenstein, Phys. Rev. B 77, 195105 (2008).
- [25] T. Paiva, R. T. Scalettar, C. Huscroft, and A. K. McMahan, Phys. Rev. B 63, 125116 (2001).
- [26] K. Mikelsons, E. Khatami, D. Galanakis, A. Macridin, J. Moreno, and M. Jarrell, Phys. Rev. B 80, 140505 (2009).
- [27] F. Werner, O. Parcollet, A. Georges, and S. R. Hassan, Phys. Rev. Lett. 95, 056401 (2005).
- [28] B. Wolf, Y. Tsui, D. Jaiswal-Nagar, U. Tutsch, A. Honecker, K. Removi-Langer, G. Hofmann, A. Prokofiev, W. Assmus, G. Donath, and M. Lang, Proceedings of the National Academy of Sciences 108, 6862 (2011).
- [29] O. A. Starykh and L. Balents, Phys. Rev. Lett. 98, 077205 (2007).
- [30] G. Li, M. Laubach, A. Fleszar, and W. Hanke, Phys. Rev. B 83, 041104 (2011).
- [31] T. Tohyama and S. Maekawa, Phys. Rev. B 67, 092509 (2003).
- [32] J. Jakli and P. Prelovek, Advances in Physics 49, 1 (2000).

- [33] B. Kumar and B. S. Shastry, Phys. Rev. B 68, 104508 (2003).
- [34] N. S. Vidhyadhiraja, A. Macridin, C. Şen, M. Jarrell, and M. Ma, Phys. Rev. Lett. 102, 206407 (2009).
- [35] M. R. Peterson and B. S. Shastry, Phys. Rev. B 82, 195105 (2010).
- [36] N. Kaurav, K. K. Wu, Y. K. Kuo, G. J. Shu, and F. C. Chou, Phys. Rev. B 79, 075105 (2009).
- [37] R. H. Mckenzie, CONDENSED CONCEPTS, http://condensedconcepts.blogspot.de.

SUPPLEMENTAL MATERIAL

The magnetic transition boundary is determined by extrapolating the spin susceptibility $\chi_{spin}(Q, \Omega_m = 0)$ with polynomials. For $\beta t \geq 7$, we look for the divergence of $\chi_{spin}^{-1}(Q, \Omega_m = 0)$ at given temperature T as a function of interaction U, as shown in the left panel of Fig. 5. For $U/t \geq 10$ we extrapolate $\chi_{spin}^{-1}(Q, \Omega_m = 0)$ for each given interaction U as a function of temperature T, see right panel of Fig. 5.

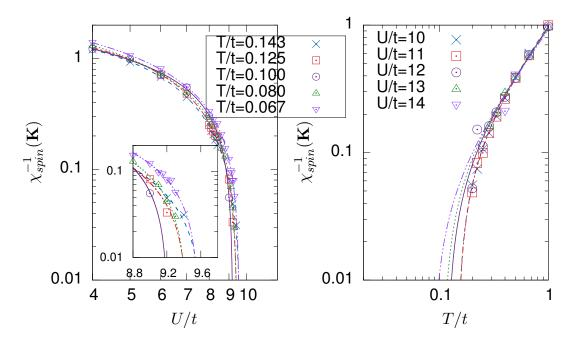


FIG. 5. Polynomial extrapolation of the inverse spin susceptibility as functions of interaction U (left panel) or temperature T (right panel).